Optics and Lasers in Engineering 85 (2016) 9–17

Contents lists available at ScienceDirect

Optics and Lasers in Engineering

journal homepage: www.elsevier.com/locate/optlaseng

Development of a compact 3D shape measurement unit using the light-source-stepping method

Motoharu Fujigaki [a,*], Toshimasa Sakaguchi [b], Yorinobu Murata [c]

[a] Graduate School of Engineering, University of Fukui, Fukui 910-8507, Japan
[b] Graduate School of Systems Engineering, Wakayama University, Wakayama 640-8510, Japan
[c] Department of Opto-Mechatronics, Faculty of Systems Engineering, Wakayama University, Wakayama 640-8510, Japan

ARTICLE INFO

Article history:
Received 19 September 2015
Received in revised form
2 April 2016
Accepted 19 April 2016
Available online 26 April 2016

Keywords:
3D shape measurement
Light-source-stepping method (LSSM)
Linear LED device
Design method
Whole-space tabulation method (WSTM)

ABSTRACT

A compact 3D shape measurement unit that uses the light-source-stepping method (LSSM) is developed. The LSSM proposed by the authors is a phase-shifting fringe projection method for shape measurement. The authors also developed a linear LED device for high-speed shape measurement using the LSSM. A compact and high-speed 3D shape measurement unit can be realized using a linear LED device. However, the LSSM is difficult to utilize because the phase-shifting amount is not uniform. The phase-shifting amount depends on the distance from the grating plate. It is therefore necessary to consider carefully the locations of the linear LED device and the grating plate. In this paper, the design method for a 3D shape measurement unit that uses the LSSM is shown, and a prototype of a compact 3D shape measurement unit with a linear LED device is developed.

1. Introduction

Accurate and high-speed 3D shape measurement systems are required for quality inspections in various industrial fields. Many researchers have studied the development of a 3D shape measurement system [1]. An LCD (liquid crystal device) and a DMD (digital micro-mirror device) are often used as fringe projection methods with phase-shifting [2,3]. Several individualistic fringe projection methods with phase-shifting have also been proposed [4–6]. Recently, these systems have also been required to be compact and inexpensive. However, most of the conventional commercialized 3D shape measurement systems are large and expensive. One of the reasons for this is that they employ imaging optics with an LCD or a DMD for phase-shifting. The response speed of an LCD is not high. A large volume is necessary for the fringe projection mechanism and imaging optics.

In contrast, the authors have proposed a light-source-stepping method (LSSM) with a linear LED device [7–9]. The projected grating phase is shifted by switching the lighting position of the linear LED light source. This linear LED device enables the shape measurement unit to be compact because a fringe projector can be assembled with a linear LED device and a grating plate. The LSSM, however, is difficult to utilize because the phase-shifting amount is not uniform. It depends on the distance of the light source from the grating plate. It is therefore necessary to develop a good method for designing a compact 3D shape measurement unit. In this paper, the design method for a 3D shape measurement is shown, and a compact 3D shape measurement device that uses the LSSM is prototyped by using this design method.

2. Light-source-stepping method (LSSM)

2.1. Ratio of phase-shifting amount

Fig. 1 shows a schematic illustration of a projected fringe pattern from a point light source and a grating plate, such as a Ronchi ruling. The grating plate is placed between the light source and the object, and a shadow of the grating plate is projected on the object. The pitch of the projected fringe pattern at position $z=0$ is represented as follows:

$$p_0 = \frac{a + z_g}{a} p_g, \tag{1}$$

where $a=(z_s-z_g)$ is the distance between the light source and the grating plate.

In reality, the light source is not a point but is instead spread spatially. Consequently, the projected pattern of the shadow of the grating plate is unsharpened as a sinusoidal pattern. The projected pattern is thus available for 3D shape measurement. The distortion of the projected pattern gives the phase error as the systematic error. However, most systematic errors can be eliminated using a

* Corresponding author.

http://dx.doi.org/10.1016/j.optlaseng.2016.04.016

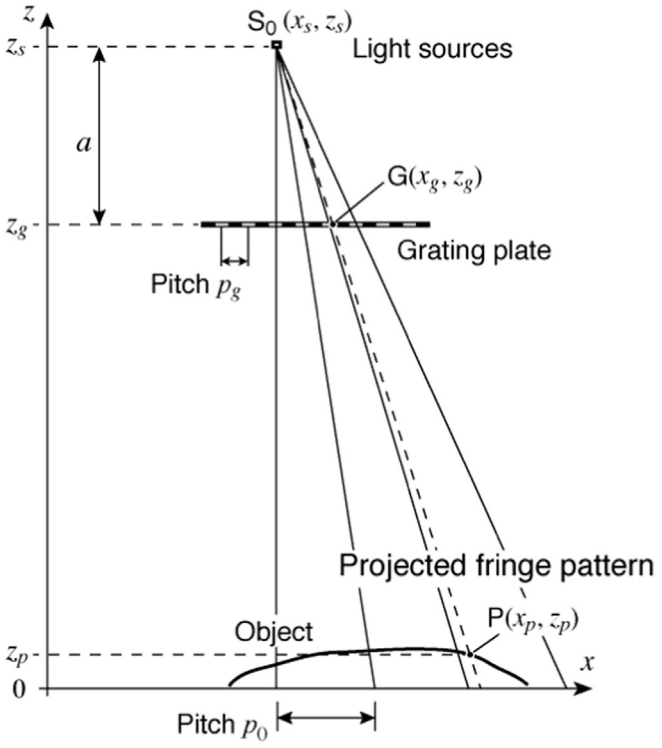

Fig. 1. Projected fringe pattern from a point light source through a grating plate.

whole-space tabulation method (WSTM) [9,10] to be described in the next section.

Fig. 2 shows the phase-shifted projected fringe patterns for three light sources: S_0, S_1, and S_2. These light sources are located at the same z position and at regular intervals of p_s, as shown in Fig. 2. When the active light source is changed from S_0 to S_1, the position of the projected fringe pattern is changed from the continuous line to the larger dashed line, as shown in Fig. 2. Similarly, when the active light source is changed from S_1 to S_2, the position of the projected fringe pattern is changed from the larger dashed line to the smaller dashed line. Therefore, the projected fringe pattern can be shifted by changing the active light source. If the light sources are LEDs, it is possible to change quickly the active light source. We call this method the light-source-stepping method (LSSM).

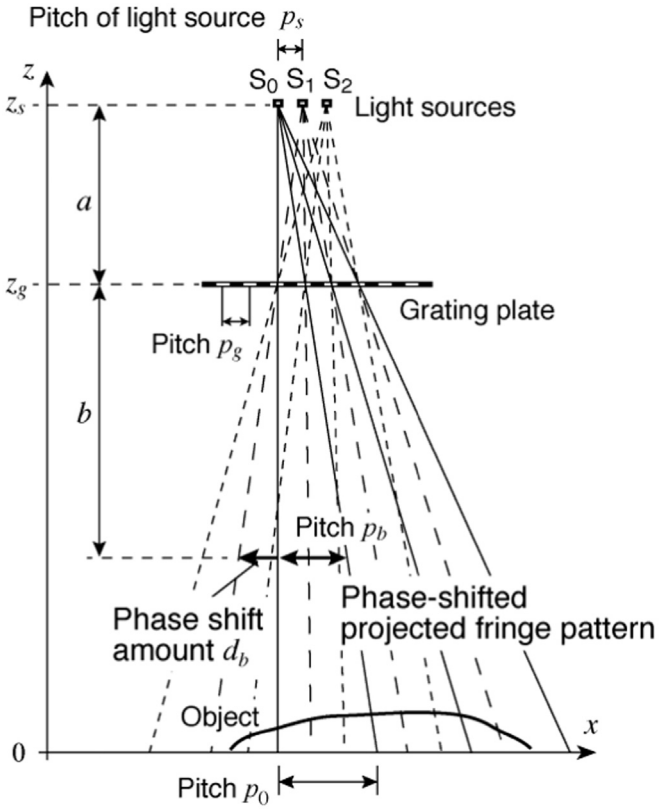

Fig. 2. Phase-shifted projected fringe pattern using the light-source-stepping method.

The projected fringe pitch p_b at $z=z_g-b$ becomes

$$p_b = \frac{a+b}{a} p_g. \tag{2}$$

The phase-shifting amount d_b at $z=z_g-b$ becomes

$$d_b = \frac{b}{a} p_s. \tag{3}$$

A ratio of phase-shifting amount to the fringe pitch at $z=z_g-b$ is defined as

$$R(b) = \frac{d_b}{p_b}. \tag{4}$$

It can be rewritten from Eqs. (2) and (3) as

$$R(b) = \frac{b p_s}{(a+b) p_g}. \tag{5}$$

Eq. (5) shows that the ratio $R(b)$ is not uniform with respect to the distance b from the grating plate. This property causes difficulty when designing a 3D shape measurement unit. Additionally, the change in this ratio will result in a systematic error. However, if the change in the ratio is not large, this systematic error can be eliminated with the WSTM. However, a larger change in the ratio will cause a large error. Therefore, this ratio is an important parameter when designing a 3D shape measurement unit as shown in the following section.

2.2. Whole-space tabulation method (WSTM)

Authors proposed a calibration method for an accurate and high-speed shape measurement using multiple reference planes. Fig. 3(a) and (b) shows the principle of the calibration method. A reference plane oriented vertically to the z-direction is translated in the z-direction by small amount. A two-dimensional grating is fixed on the reference planes as shown in Fig. 3(b). A fringe pattern generated with a light source and a grating plate is projected onto the reference planes and an object. The phase of the projected fringe patterns can be easily obtained using the phase-shifting method using the LSSM mentioned above.

A pixel of the camera obtains an image along the ray line L shown in Fig. 3(a). The pixel contains images of points P_0, P_1, P_2…P_N on reference planes R_0, R_1, R_2…R_N, respectively. At each point, grating phases θ_0, θ_1, θ_2…θ_N can be calculated using the phase-shifting method. Therefore, the correspondence between heights z_0, z_1, z_2…z_N and phases θ_0, θ_1, θ_2…θ_N, respectively, is obtained with one-to-one relationship. A calibration table between phase θ and the z-coordinate can be formed as shown in Fig. 4(c). The table elements are obtained by a linear interpolation at a regular interval for phase θ.

The x-and y-coordinates of points P_0, P_1, P_2…P_N are also obtained from the two-dimensional grating fixed on the reference planes located at z_0, z_1, z_2…z_N, respectively, as shown in Fig. 3(b). The x-and y-coordinates can be obtained accurately using a phase-analysis method such as the Fourier transform method and phase-

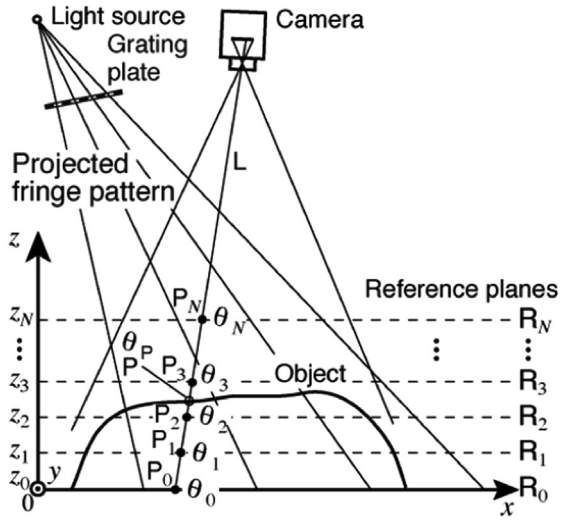

(a) z-coordinates corresponding to the phase θ of the projected grating on a pixel line

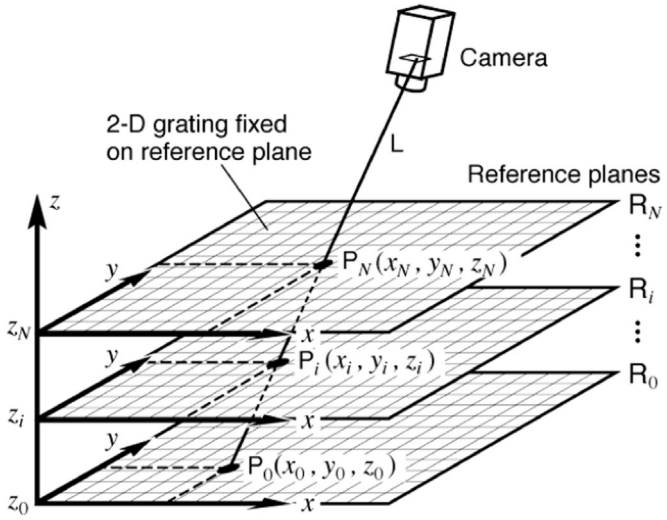

(b) The x- and y-coordinates corresponding to the z-coordinate on a pixel line

Fig. 3. Principle of calibration method using WSTM.

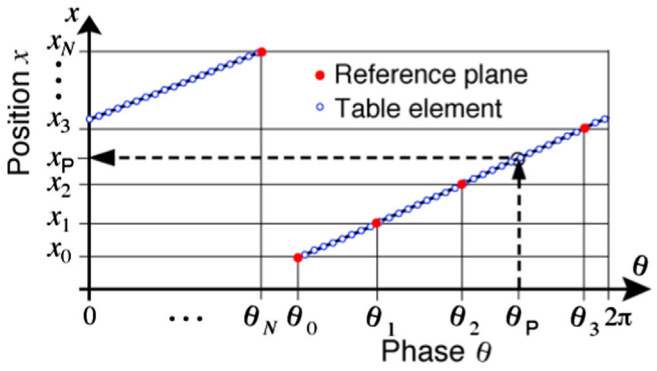

(a) Table of phase θ and x-coordinate

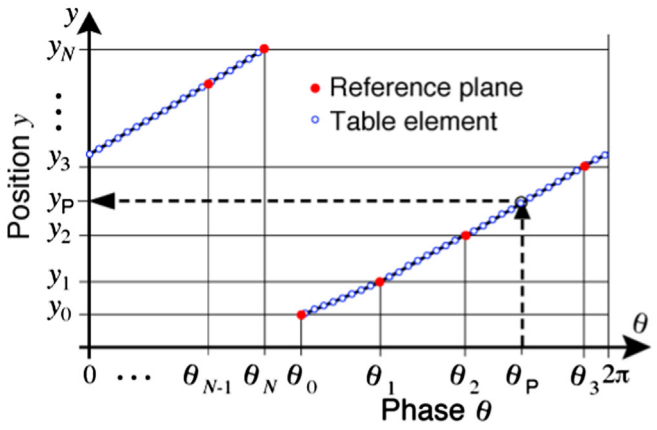

(b) Table of phase θ and y-coordinate

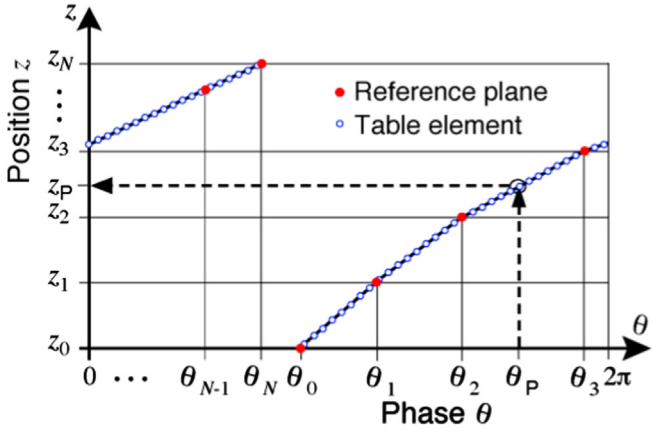

(c) Table of phase θ and z-coordinate

Fig. 4. Schema of calibration tables to obtain x-, y-, and z-coordinates from phase θ of the projected grating on a pixel line.

shifting method. A calibration table between phase θ and the x-coordinate and a calibration table between phase θ and the y-coordinate can be also formed as shown in Fig. 4(a) and (b), respectively. The table elements are also obtained by a linear interpolation at a regular interval for phase θ.

After producing these calibration tables, an object is placed between reference planes R_0 and R_N as shown in Fig. 3(a). When the phase at point P, which is an intersectional point between the ray line L and the surface of the object, is $\theta_{\square}$, The x-, y-and z-coordinates can be obtained immediately from the calibration tables shown in Fig. 4(a), (b) and (c), respectively.

2.3. Error propagation from phase to coordinates

The standard deviation of z-coordinate σ_z is obtained as

$$\sigma_z^2 = a^2\sigma_\theta^2 \quad \left(a = \frac{dz}{d\theta}\right), \tag{6}$$

according to the law of error propagation, where σ_θ is a standard deviation of phase θ and a is a gradient on the relationship between the phase θ and the z-coordinate. It can be rewritten from Eq. (6) as

$$\sigma_z = a\sigma_\theta. \tag{7}$$

Fig. 5 shows a relationship between the gradient and the

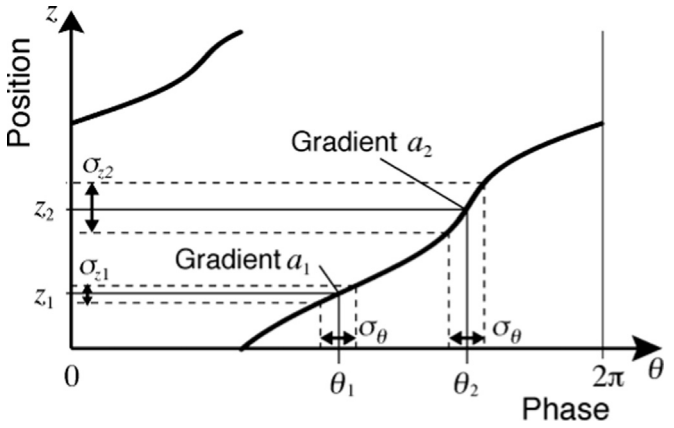

Fig. 5. Relationship between the gradient and the standard deviation of z-coordinate on a table of phase θ and z-coordinate.

standard deviation of z-coordinate on a table of phase θ and z-coordinate. In this figure, the gradient a_1 is smaller than the gradient a_2. In this case, the standard deviation σ_{z1} becomes smaller than the standard deviation σ_{z2} when both the standard deviation of θ_1 and θ_2 is σ_θ. The gradient is, therefore, an important factor to consider the accuracy when designing a 3D shape measurement unit using the WSTM.

2.4. Relationship between initial phase and analyzed phase

The gradient change mentioned above is caused by an arrangement of optical setup, an intensity profile of the projected grating distorted from a sinusoidal pattern, the phase-shifting error from the ideal phase-shifting amount, and so on. The main cause of the gradient change is the phase-shifting error. Relationship between initial phase and analyzed phase with various ratio of phase-shifting amount is, therefore, simulated in this

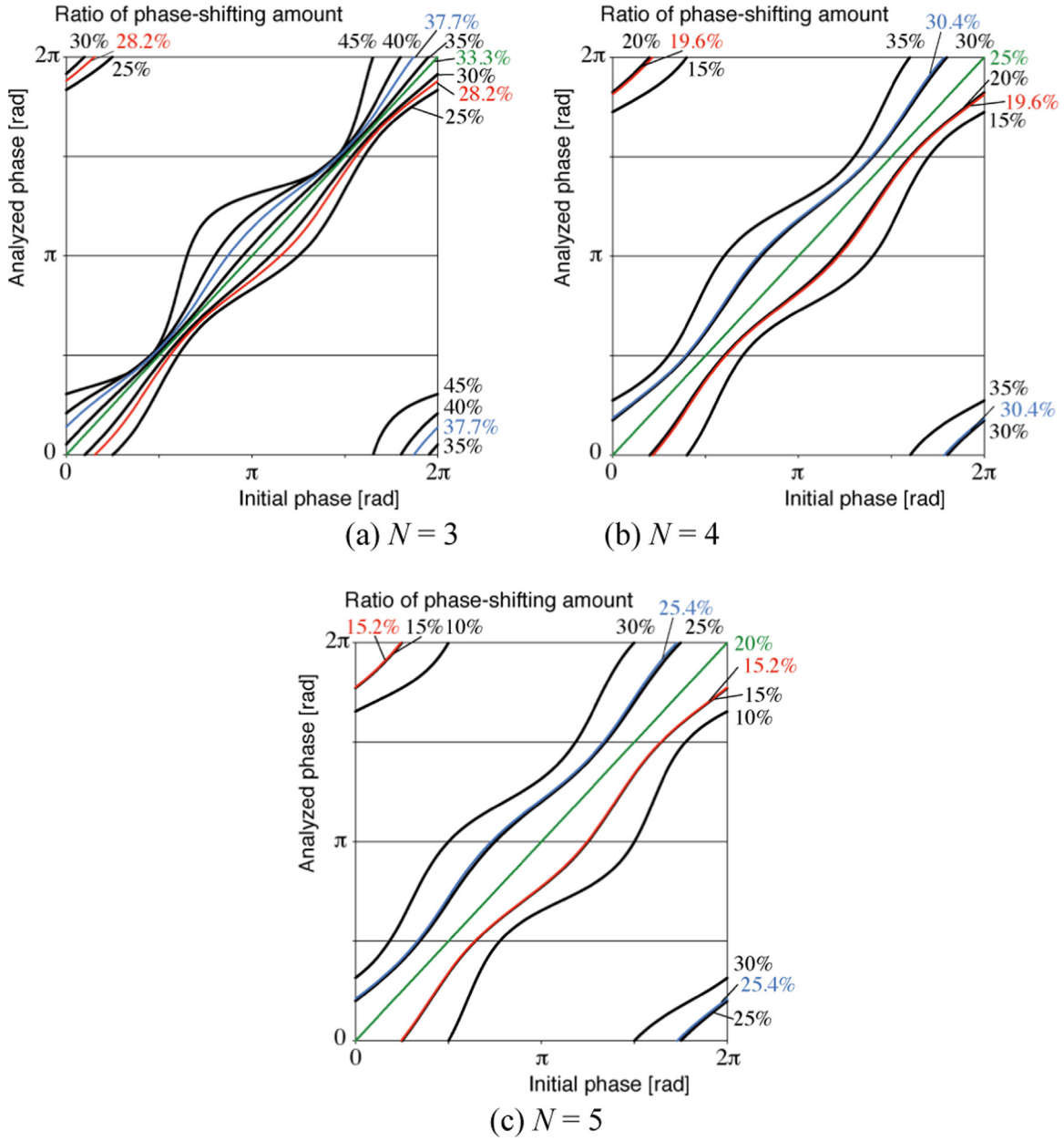

Fig. 6. Relationship between initial phase and analyzed phase with various ratio of phase-shifting amount. (For interpretation of the references to color in this figure, the reader is referred to the web version of this article.)

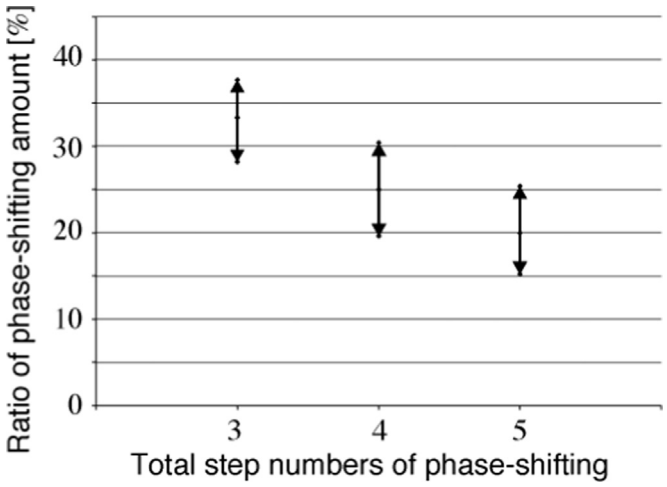

Fig. 7. Range of ratio of phase-shifting amount under the condition that the ratio of the maximum gradient and the minimum gradient is less than 2.

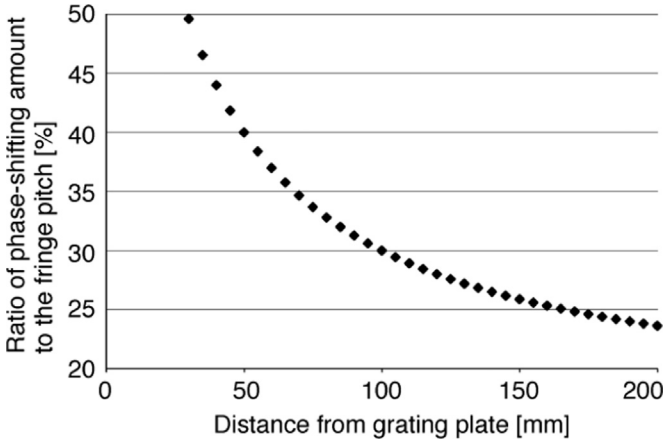

Fig. 8. Ratio of phase-shifting amount against a pitch of projected fringe pattern.

section. In this simulation, N-step phase-shifting method is employed. Intensities I_k at each initial phase θ_0 are defined as,

$$I_k = \cos(\theta_0 + 2\pi Rk), \tag{8}$$

where k is an integer number between 0 and $N-1$ and R is a ratio of phase-shifting amount. The analyzed phase θ is calculated using the discrete Fourier transform (DFT) algorithm. The relationship between the analyzed phase θ and intensities I_k is expressed in,

$$\tan\theta = -\frac{\sum_{k=0}^{N-1} I_k \sin\left(k\frac{2\pi}{N}\right)}{\sum_{k=0}^{N-1} I_k \cos\left(k\frac{2\pi}{N}\right)}, \tag{9}$$

where k is an integer number between 0 and $N-1$ and I_k are intensities obtained at a pixel with N-step phase-shifting.

The results of the simulation of relationship between initial phase and analyzed phase with various ratio of phase-shifting amount in the cases of $N=3$, $N=4$ and $N=5$, are shown in Fig. 6 (a)–(c), respectively. When a ratio of phase-shifting amount is $1/N$, the analyzed phases are changing as a line against the initial phase as shown as green lines in Fig. 6(a)–(c). However, when a ratio of phase-shifting amount is different from $1/N$, the analyzed phases are changing with curving against the initial phase. Black curved lines in Fig. 6(a), (b) and (c) are shown the analyzed phases in the cases that the ratio of phase-shifting amount are 10%, 15%, 20%, 25%, 30%, 35%, 40% and 45%. In these cases, the gradient at each initial phase is changed with corresponding to the initial phase.

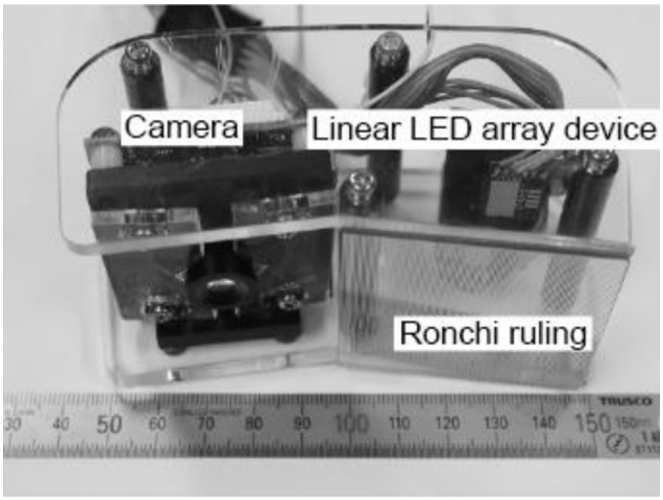

(a) Photograph

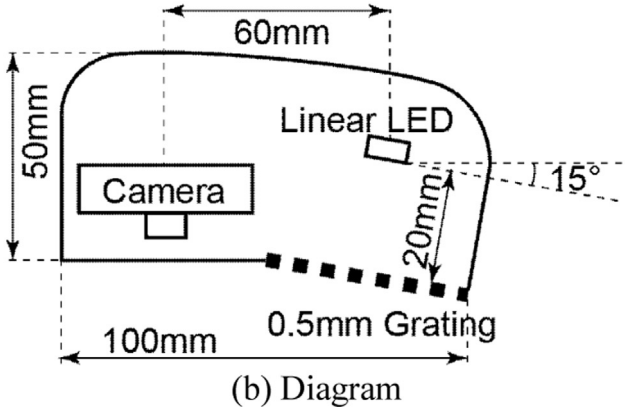

(b) Diagram

Fig. 9. Developed compact 3D shape measurement unit.

In the case of the WSTM [9,10], a phase and the z-coordinate table at each pixel is prepared in the calibration process. The z-coordinate of the measured object at each pixel is obtained from the phase of the pixel using the phase and 3D coordinate table. When the gradient of the z-coordinate against the phase is small, the standard deviation of the z-coordinate becomes small according to the law of propagation of errors. In the case of the LSSM, a large gradient of an analyzed phase against the initial phase makes a small gradient of the z-coordinate against the analyzed phase. Therefore, the gradient is corresponded to the accuracy of the 3D shape measurement.

Unevenness of the gradient at each initial phase gives unevenness of the accuracy. It is better for the 3D shape measurement that the unevenness is small. The ratio of the maximum gradient and the minimum gradient is considered in the case that the allowable ratio is less than 2. The ratio on $N=3$ becomes 2 when $R=28.2\%$ and $R=37.7\%$ as shown as a red line and a blue line in Fig. 5(a), respectively. The ratio on $N=4$ becomes 2 when $R=19.6\%$ and $R=30.4\%$ as shown as a red line and a blue line in Fig. 6(b), respectively. The ratio on $N=5$ becomes 2 when $R=15.2\%$ and $R=25.4\%$ as shown as a red line and a blue line in Fig. 6(c), respectively.

These are summarized in Fig. 4. The ranges of ratio of phase-shifting amount under the condition that the ratio of the maximum gradient and the minimum gradient is less than 2 are indicated by double-headed arrows in Fig. 7.

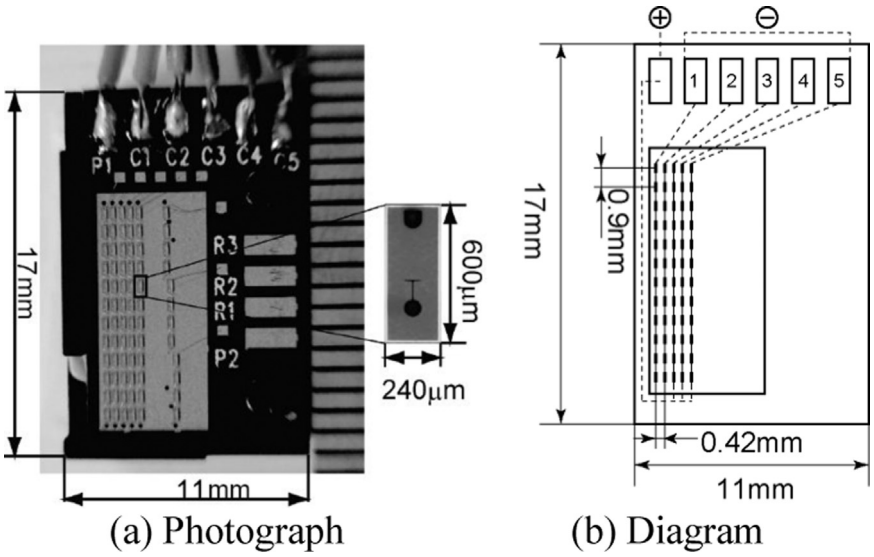

Fig. 10. Linear LED device.

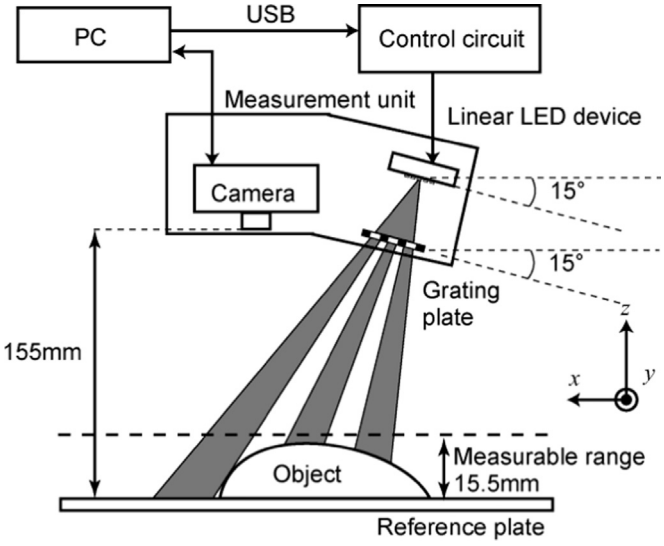

Fig. 11. Measurement system.

Fig. 12. Photograph of the reference plate and the 3D shape measurement unit.

Table 1
Measurement conditions.

Number of the phase-shifting	4
Step distance of the reference plate	0.4 mm
Number of the captured reference plate	50
Measurement x range	135 mm
Measurement y range	110 mm
Measurement z range (z_{range})	15.5 mm
Captured image size	640 × 512 pixels
Image averaging number	9
LED device current	30.0 mA

Table 2
Measurement results of a reference plate.

Given z-position [mm]	2.00	4.00	6.00	8.00	10.00
Measured height [mm]	1.99	3.99	6.00	8.00	10.00
Measurement error [mm]	0.01	0.01	0.00	0.00	0.00
Standard deviation [mm]	0.016	0.016	0.016	0.016	0.015

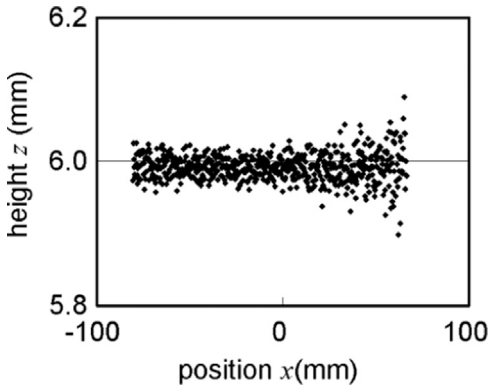

Fig. 13. Height distribution along the horizontal line at the 6 mm plate position.

3. Development of the portable 3D shape measurement unit

3.1. Design for a 3D shape measurement unit using the LSSM

The projected fringe pitch on the object and the phase-shifting amount for one step depend on the distance from the grating plate to the object. To improve the accuracy, the total step numbers of

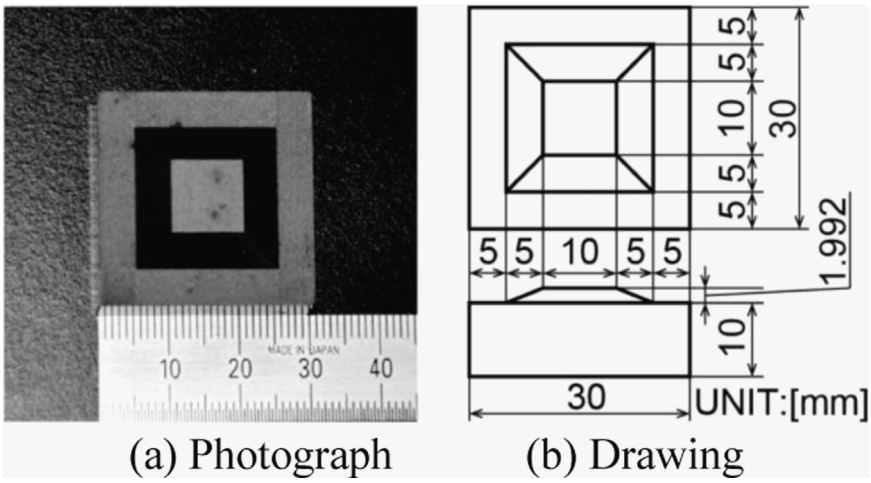

Fig. 14. Steel trapezoidal object photo and dimensions.

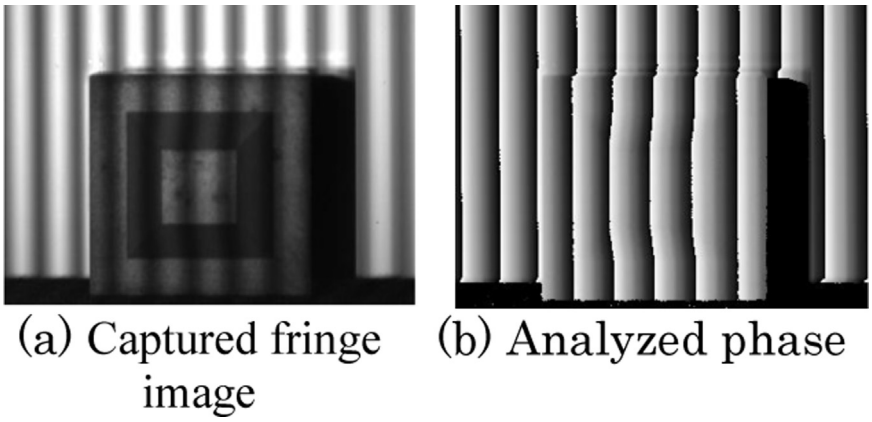

Fig. 15. Captured object images.

phase-shifting for a period can be selected as a function of the measurement conditions.

In this simulation, the grating plate is placed at $z_g=0$ mm, and the LED device is placed at $z_s=20$ mm with a distance of $a=20$ mm between the grating plate and the LED device. The pitch of the grating plate p_g is 0.5 mm, and the pitch of the LED lines p_s is 0.42 mm. Fig. 8 shows that the ratio is varied near 25% when the distance b is changed near 165 mm. Fig. 4 shows that the appropriate shift number is 4 when the ratio is changed near 25%. Therefore, the appropriate shift number for this system is 4 at $b=165$ mm. The projected fringe pitch p_0 is calculated using Eq. (5) to be 4.63 mm at this position.

3.2. Compact 3D shape measurement unit

A compact 3D shape measurement unit is produced using a linear LED device. Fig. 9(a) and (b) show a photograph and a diagram of these devices, respectively. The construction of the developed 3D shape measurement unit is very simple because it is assembled from only a board type CMOS camera, a linear LED device and a Ronchi ruling.

A board type camera (UI-5241LE-NIR, IDS Imaging Development Systems GmbH) with an S-mount lens is employed in the 3D shape measurement unit. The size of the camera is 45 mm × 45 mm, and the imaging sensor has 1280 × 1024 pixels.

Fig. 10 (a) and (b) shows the developed linear LED device. The size of the LED chip is 240 μm × 600 μm. This linear LED device has 5 vertical lines with pitches of 0.42 mm. Each line has 12 LED chips aligned at intervals of 0.9 mm, and the anodes of the LED lines are connected to a common electrode. The center wavelength of the emitted light is 448 nm, and the half width at half maximum is approximately 10 nm. The size of the substrate mounted on the aluminum base block is 11 mm × 17 mm.

The size of the Ronchi ruling is 50.8 mm × 50.8 mm, and the pitch is 0.5 mm. The normal directions of the linear LED device and the Ronchi ruling are adjusted by 15° from the optical axis of the camera. The linear LED device is located at a distance of 20 mm from the Ronchi ruling.

4. Experiments for evaluation

Fig. 11 shows the measurement setup. The control circuit consists of a microcomputer and a driver for the linear LED device. The timing of the changing lighting of the LED lines is controlled by the microcomputer.

An LCD display with a diffusing sheet attached on the surface is used as a reference plate. Fig. 12 shows a photograph of the reference plate and the 3D shape measurement unit projecting a fringe pattern onto the reference plate. The reference plate is located on a moving stage. The normal direction of the surface is adjusted to the moving direction of the stage. The reference plate is used to generate the calibration tables of the relationship between the coordinates and the phase of the projected fringe pattern. A calibration table is generated for each camera pixel.

Table 1 shows the summarized measurement conditions for the experiments. Four is used as the number of the phase-shifting because the ratio of the phase-shifting against a pitch of projected

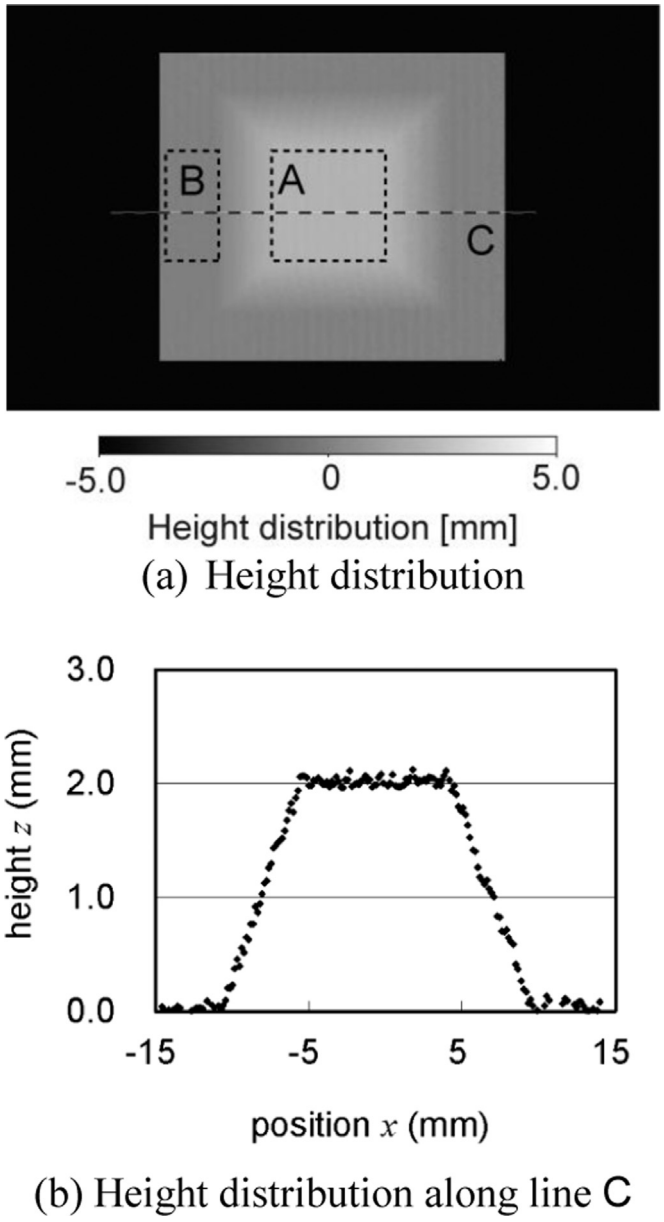

Fig. 16. Trapezoidal object measurement results.

Table 3
Trapezoidal object measurement results.

	Average of height z [mm]	Standard deviation [mm]
Area A	2.02	0.040
Area B	0.02	0.050
Difference	2.00	–
Error	0.00	–

fringe is approximately 25% in this condition according to the simulation mentioned above. The step distance of the reference plate is 0.4 mm, and the phase-shifting number of the captured reference plate is 50. The effective measurement range for the z-direction is 15 mm for this case.

4.1. Flat plate

First, the reference plate, which is shown in Fig. 12, was measured by considering it to be a flat plate specimen. The position of the flat plate is located by the moving stage with a 0.01 mm positioning resolution.

Table 2 gives the average height distributions and errors between the plate positions and the measured results. Fig. 10 shows the height distribution along the central horizontal line in the measurement area at the $z=6.00$ mm plate position. These results show that the measured error is less than 0.01 mm and that the standard deviation is less than 0.02 mm. The standard deviations at each position are almost the same. In addition, Fig. 13 shows that the measured height has no distortion according to the features of the WSTM.

It is expected that the measured results are at the best condition because the object and the reference plate used to generate the table of the relationship between the coordinates and the phase are the same. The principal reason for the dispersion in the results at the measured height is the random noise contained in the captured images.

4.2. Measuring a steel trapezoidal object

Second, a steel trapezoidal object, which is shown in Fig. 14, is measured. This shape was machined by electrical discharge machining. The height of the center part of the object is 1.992 mm and is measured by a microscopic height gauge.

Fig. 15 shows a captured fringe image and the analyzed phase. Fig. 16(a) shows the analyzed height distribution, and Fig. 16(b) shows the height distribution along the line C in Fig. 16(a). Table 3 shows the average heights and standard deviations of areas A and B in Fig. 16(a). The measurement error for the height of the center part is less than 0.01 mm. The standard deviations of areas A and B are under 0.05 mm. No distortion appears in these results.

A standard deviation of approximately 4 times of the flat plate appears in the measurement results for the trapezoidal object. The random noise contained in these captured images is almost the same for the trapezoidal object as they are for the flat plate. However, the reflectance of the surface is lower than that of the flat plate. A small unevenness in the surface is one of the reasons for the larger standard deviation.

Regarding the error and distortion, a small error under 0.01 mm with no distortion appears in both cases. The accuracy of this 3D shape measurement unit is at a comparable level with conventional 3D shape measurement devices.

5. Conclusions

A design method for 3D shape measurement was shown. It was shown that the ratio of the phase-shifting amount to the fringe pitch was an important parameter to the design of a 3D shape measurement unit using the LSSM. The distance between a linear LED device and a grating plate on a compact 3D shape measurement unit and the measurement range were designed using the ratio of the phase-shifting amount to the fringe pitch. A compact 3D shape measurement unit can be realized using this design method. The accuracies of the results from the experiment to measure a flat plate and a steel trapezoidal object were less than 0.01 mm and 0.02 mm, respectively.

Acknowledgment

This research is partially supported by the Japan Science and Technology Agency (JST), Japan, A-STEP Program (Grant number: AS2414111H).

References

[1] Gorthi SS, Rastogi P. Fringe projection techniques: whither we are? Opt Lasers Eng 2010;48(2):133–40.
[2] Yen HN, Tsai DM, Yang JY. Full-field 3-D measurement of solder pastes using LCD-based phase shifting techniques. IEEE Trans Electron Packag Manuf 2006;29(1):50–7.
[3] Gong Y, Zhang S. Ultrafast 3-D shape measurement with an off-the-shelf DLP projector. Opt Express 2010;18(19):19743–54.
[4] Yoshizawa T, Wakayama T, Takano H. Application of a MEMS scanner to profile measurement. In: Proceedings of the SPIE 2007;6762:67620B-1-5.
[5] Zwick S, Fessler R, Jegorov J, Notni G. Resolution limitations for tailored picture-generating freeform surfaces. Opt Express 2012;20(4):3642–53.
[6] Grosse M, Schaffer M, Harendt B, Kowarschik R. Fast data acquisition for three-dimensional shape measurement using fixed-pattern projection and temporal coding. Opt Eng 2011;50(10) 100503-1.
[7] Oura Y, Fujigaki M, Masaya A, Morimoto Y. Development of linear LED device for shape measurement by light source stepping method, optical measurements. Model Metrol 2011;5:285–91.
[8] Morimoto Y, Masaya A, Fujigaki M, Asai D. Shape measurement by phase-stepping method using multi-line LEDs. In: Zahurul Haq Md, editor. Applied measurement systems. InTech; 2012. p. 137–52 Chapter 7.
[9] Fujigaki M, Oura Y, Asai D, Murata Y. High-speed height measurement by a light-source-stepping method using a linear LED array. Opt Express 2013;21(20):23169–80.
[10] Fujigaki M, Morimoto Y. Shape measurement with grating projection using whole-space tabulation method. J JSEM (Jpn) 2008;8–4:402–8.